Science of Sintering, **48** (2016) 1-16

doi: 10.2298/SOS1601001C

UDK 669.018; 676.017.5

Synthesis, Structure and Properties of Nickel-Iron-Tungsten Alloy Electrodeposits
PART II: Effect of Microstructure on Hardness, Electrical and Magnetic Properties

Nataša Ćirović[1*)], Pavle Spasojević[1,3], Lenka Ribić-Zelenović[2*)], Pavle Mašković[2], Aleksa Maričič[3], Miroslav Spasojević[2,3]

[1]Faculty of Technology and Metallurgy, University of Belgrade, Belgrade, Serbia
[2]Faculty of Agronomy, Čačak, University of Kragujevac, Čačak, Serbia
[3]Joint Laboratory for Advanced Materials of SASA, Section for Amorphous Systems, Faculty of Technical Sciences, Čačak, University of Kragujevac, Čačak, Serbia

Abstract:

Nanostructured nickel-iron-tungsten alloys were produced by electrodeposition from an ammoniacal citrate bath. The tungsten content of the alloy ranged from 0.8 wt.% to 11 wt.%, and the crystal grain size of the FCC phase of the solid solution of iron and tungsten in nickel was between 14 nm and 3.3 nm. The amorphous phase content of the alloy increases with decreasing crystal grain size. As the amorphous phase content increases, the magnetization, electrical conductivity and hardness of the alloy decrease. Annealing the alloy to crystallization temperature results in structural relaxation during which the alloy undergoes short-range ordering in conjunction with decreases in the density of chaotically distributed dislocations and internal microstrain level, which increases the exchange integral value, the electronic density of states at the Fermi level, the mean free path of electrons, the ordering and the mean size of cluster in the sliding plane and results in more uniform orientation of dipole moments of certain nanoparticles. These changes: a) increase the mobility of magnetic domain walls, facilitate the orientation of domains in the external magnetic field and cause an increase in magnetization; b) cause a decrease in electrical resistance, and c) impede the sliding of grain boundaries and increase the hardness of the alloy.

Annealing the alloys at temperatures above 400ºC results in amorphous phase crystallization and larger crystal grains of the FCC phase, along with a decrease in the density of chaotically distributed dislocations and a decrease in internal microstrain level.

The formation of larger crystal grains reduces the hardness of the alloy, decreases its specific electrical resistance and impedes both the orientation of certain magnetic domains and the shift of walls of already oriented domains, thus inducing a decrease in magnetization.

The heat released during the milling of $Ni_{87.3}Fe_{11.3}W_{1.4}$ alloy with FCC-phase crystal grains 8.8 nm in average size causes amorphous phase crystallization, FCC crystal grain growth and an increase in magnetization.

Alloys with relatively high tungsten content (11 wt. %) have an inhomogeneous composition, a high proportion of the amorphous phase and FCC crystal grains with an average size of 3.3 nm. This microstructure results in magnetic domains that have different and relatively low thermal stabilities and relatively low degrees of magnetization.

Keywords*: Nanostructured alloy, FCC phase, Electrical resistance, Magnetization.*

*) **Corresponding authors**: cirovic@ptt.rs, lenka@kg.ac.rs

1. Introduction

Nanocrystalline nickel-iron-tungsten alloys have good electrical, magnetic and mechanical properties, high thermal stability and high corrosion resistance. Therefore, they are extensively used in novel technologies, generally as materials for microelectronics and microelectromechanical systems and as cathodes for hydrogen evolution [1-18]. More recently, relatively inexpensive electrochemical procedures have been developed for the fabrication of these alloys from environmentally friendly citrate ammonia solutions without any environmental and health risks [2, 9, 15, 17, 18]. Electrodeposition can result in alloys whose microstructure and physicochemical properties are different from those of metallurgically prepared alloys having the same chemical composition. The properties of electrochemically generated alloys are dependent on the kinetic and operating parameters of electrolysis [19-28]. Tungsten and molybdenum can be electrodeposited only with iron group metals [2, 29-33]. The mechanism of codeposition of these metals and the effect of electrolysis parameters on the chemical composition, microstructure, morphology and physicochemical properties have been examined in a number of studies [17, 24-37].

Amorphous and nanocrystalline alloys occur in a metastable state. Annealing at elevated temperatures and milling cause changes in their microstructure and morphology, thus affecting their magnetic, electrical and mechanical properties, catalytic activity, corrosion resistance and thermal stability [38-42]. At temperatures below the crystallization temperature, the alloys undergo structural relaxation, whereas amorphous phase crystallization and nanocrystal grain growth take place at higher temperatures [38-42].

The objective of this paper was to present a review of research conducted under the Project Ref. No. 172057 funded by the Ministry of Education and Science of the Republic of Serbia. Part I presents the effect of synthesis parameters on the chemical composition, microstructure and morphology of nickel-iron-tungsten alloy electrodeposits. Part II shows the effect of the chemical composition and microstructure on the magnetic and electrical properties and hardness of the electrodeposited nickel-iron-tungsten alloy.

2. Experimental

Nickel-iron-tungsten alloys were electrodeposited on copper, mild steel and titanium cathodes. During the measurement, a standard electrical circuit and a glass electrochemical cell were used. The alloys were produced by the electrolysis of solutions A and B of the following compositions:

Solution A	Solution B
0.2 mol dm^{-3} $NiSO_4•6H_2O$	0.012 mol dm^{-3} $NiSO_4•6H_2O$
0.02 mol dm^{-3} $FeSO_4$	0.004 mol dm^{-3} $FeSO_4$
0.004 mol dm^{-3} $Na_2WO_4•2H_2O$	0.01 mol dm^{-3} $Na_2WO_4•2H_2O$
0.24 mol dm^{-3} $Na_3C_6H_5O_7•2H_2O$	0.06 mol dm^{-3} $Na_3C_6H_5O_7•2H_2O$
0.8 mol dm^{-3} NH_4Cl	0.5 mol dm^{-3} NH_4Cl
0.3 mol dm^{-3} Na_2SO_4	1.0 mol dm^{-3} H_3BO_3
pH=9.2±0.1	0.15 mol dm^{-3} NaBr
	pH=9.2±0.1
t = 65±0.5ºC	t = 50±0.5ºC; 60±0.5ºC and 70±0.5ºC

The chemical composition of the alloys was determined by energy dispersive X-ray spectroscopy (EDS) and by atomic absorption. Scanning electron microscopy (SEM) was

used to determine the morphology of the electrodeposits. The microstructure of the electrodeposits was evaluated by X-ray analysis. The size and shape of powder particles were analyzed by a Leica Q500MC. The as-prepared alloys were milled in an alcohol medium using a planetary ball mill.

Magnetization measurements were performed by a modified Maxwell method, based on the action of an inhomogeneous field on the magnetic sample. Magnetic force measurements were carried out with a sensitivity of 10^{-6} N in an argon atmosphere.

The electrical properties of the electrodeposits were investigated using 40 mm x 1.2 mm x 0.5 mm samples obtained by exposing the deposits to a pressure of 100 MPa. Electrical resistivity was measured by the four-point method.

Hardness was measured using the samples on Cu and Fe substrates with a 0.002 kg load and loading time of 15 s in cross section. Each value was the average of five readings.

3. Results and discussion

Part I shows that the parameters involved in the electrodeposition and subsequent treatment of the nickel-iron-tungsten alloys determine their chemical composition, microstructure and morphology. The effect of these characteristics on the magnetic, electrical and mechanical properties of the alloys was analyzed in this part (Part II).

Fig. 1. presents the magnetization of the as-produced coatings obtained from solution A as a function of mean crystallite size of the FCC phase of the solid solution of iron and tungsten in nickel. As shown in the diagram, magnetization increases with increasing mean crystallite size from 8.8 nm to 14.0 nm. The increase in magnetization is due to a reduction in the proportion of the amorphous phase and due to a decrease in the density of chaotically distributed dislocations.

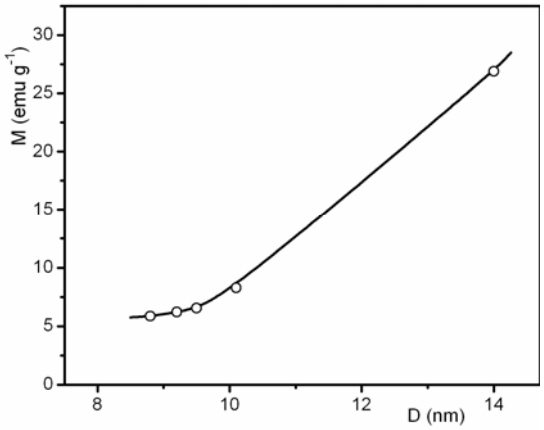

Fig. 1. Magnetization of the as-prepared coatings at 25ºC obtained by electrolysis from solution A as a function of mean crystallite size.

The density of chaotically distributed dislocations in both phases and the mean crystallite size of the FCC phase of the solid solution of iron and tungsten in nickel can change after annealing at elevated temperatures. Annealing the alloy at t<400ºC induces structural relaxation accompanied by a decrease in the minimum density of chaotically distributed dislocations and a reduction in the mean internal microstrain value, leading to changes in magnetization (Fig. 2).

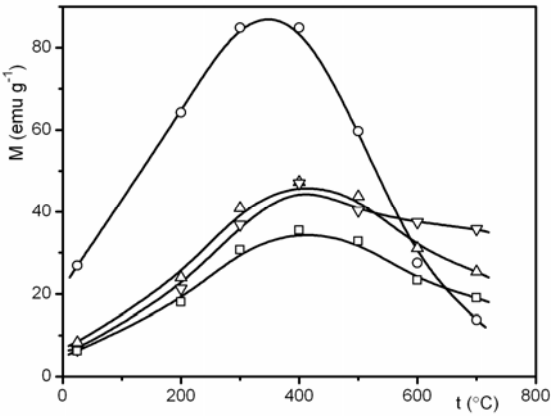

Fig. 2. Magnetization of the coatings cooled at 25ºC as a function of annealing temperature and deposition current density: ○- 50 mAcm^{-2}; Δ - 100 mAcm^{-2}; ∇ – 200 mAcm^{-2}; □ – 300 mAcm^{-2}. The coatings were obtained by electrodeposition from solution A.

Fig. 2. presents the magnetization of the coatings cooled at 25ºC and pre-annealed for 30 minutes at specified elevated temperatures. As shown in the Fig., magnetization increases with increasing annealing temperature to about 400ºC. A further increase in temperature leads to a decrease in magnetization. The increase in magnetization after annealing to 400ºC is due to structural relaxation. Electrodeposition does not result in an amorphous phase with a completely random distribution of distances between neighboring atoms. No ideal amorphous phase is formed; rather, a phase with short-range order exhibited to a greater or lesser extent [43, 44]. Moreover, electrodeposition results in an FCC phase with the density of chaotically distributed dislocations and internal microstrain levels present to a greater or lesser extent. The proportion of the amorphous phase, the mean crystallite size of the FCC phase and the degree of order of both phases are dependent on the deposition current density. As the deposition current density increases, the proportion of the amorphous phase is increased and its short-range order is decreased. The mean size of FCC crystallites is decreased, and the minimum density of chaotically distributed dislocations is increased. During annealing to 400ºC, structural relaxation takes place in the alloy. The effect of thermal energy in the amorphous phase results in short-range ordering of the structure. Also, the FCC phase undergoes partial short-range ordering of the structure, with a simultaneous decrease in the minimum density of chaotically distributed dislocations and internal microstrain levels. Through the thermal energy effect, certain atoms located at higher energy levels cross energy barriers and reach lower energy levels. At these lower levels, their 3d and 4s orbitals overlap more effectively with the same type of orbitals of neighboring atoms, thus increasing the values of the exchange integral and the electron density of states at the Fermi level [13, 14, 22-26, 28, 43, 44]. Short-range ordering also leads to an increase in the mean free path of electrons [13, 14, 22-26, 28, 43, 44]. Then, the atoms arriving at lower energy levels adjoin the energetically more favorable domain. The lower density of chaotically distributed dislocations, upon structural relaxation, enhances the mobility of magnetic domain walls and facilitates the orientation of these domains in the external magnetic field. These changes enable magnetic domain expansion and, hence, an increase in magnetization. [13-16, 22-26, 28, 33, 42, 45]

Magnetization decreases as annealing temperature increases in the temperature range between 400ºC and 700ºC. The decrease in magnetization is due to the formation of larger crystal grains of the FCC phase through amorphous phase crystallization. Large sized crystal grains impede the orientation of certain magnetic domains and reduce the shift of walls of already oriented domains [13, 14, 22-26, 28, 33, 42, 45].

The as-prepared coatings contain an amorphous phase exhibiting a relatively low degree of magnetization, and an FCC phase containing small grains, which shows a relatively higher degree of magnetization. Total magnetization depends on the proportion of these phases in the coatings. The magnetization of the as-prepared coatings deposited at 50 $mAcm^{-2}$ is over three times the magnetization of the as-prepared coatings deposited at current densities above 100 $mAcm^{-2}$ (Figs. 1 and 2). This finding confirms that these coatings have a considerably smaller proportion of the amorphous phases compared to those deposited at higher current densities (j>100 $mAcm^{-2}$). During annealing at 400ºC, the magnetization of the coatings deposited at 50 $mAcm^{-2}$ is increased by 3.16 times, and that of the coatings deposited in the current density range of 100 to 300 $mAcm^{-2}$ by 5.7 to 7.1 times. The coatings deposited at 50 $mAcm^{-2}$ have the lowest content of the amorphous phase exhibiting the highest degree of short-range ordering and the lowest density of chaotically distributed dislocations in the crystalline FCC phase. Therefore, during relaxation, the smallest structural changes and, hence, the smallest relative increase in magnetization occur in these coatings. The coatings obtained at j ≥100 $mAcm^{-2}$ have less ordered amorphous and FCC phases and, therefore, they undergo larger short-range structural changes during annealing at 400ºC. As a result, structural relaxation in these coatings causes a higher relative increase in magnetization. The increase in magnetization during the structural relaxation at 400ºC in the coatings deposited at 50 $mAcm^{-2}$ is mostly attributed to changes in the FCC phase. Therefore, the increase in the absolute value of magnetization is the highest in these coatings.

Fig. 3. presents the magnetization of the coatings obtained by electrolysis from solution A as a function of mean crystallite size and annealing temperature.

The diagrams presented in Fig.s 1, 2 and 3 suggest that the increase in magnetization causes: a) a reduction in the amorphous phase content; b) a decrease in mean FCC crystal size, and c) an increase in short-range ordering in both phases. The increase in the magnetization of the coatings obtained at the current densities between 50 and 300 $mAcm^{-2}$ is dominantly induced by the decrease in amorphous phase content with decreasing deposition current density. The change in the magnetization of these coatings during annealing at temperatures below 450ºC is dominantly affected by short-range ordering and that at temperatures above 500ºC by amorphous phase crystallization and the formation of larger crystal grains of the FCC phase.

Milling and annealing the as-prepared electrodeposit change its microstructure and, hence, its magnetic properties. Electrodeposition from solution A at a current density of j = 500 $mAcm^{-2}$ results in the formation of $Ni_{87.3}Fe_{11.3}W_{1.4}$ alloy powder with a mean particle size of 153.01μm and a mean crystal size of 8.8 nm.

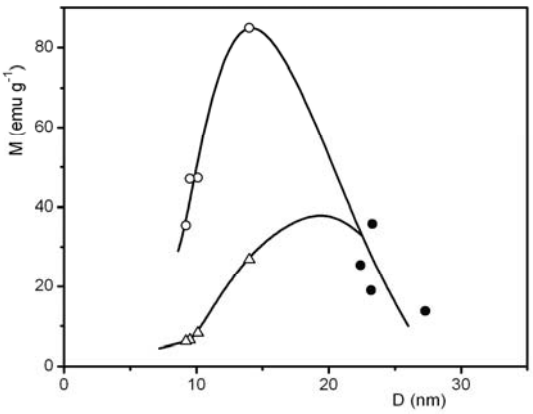

Fig. 3. Magnetization of the coatings cooled at 25ºC as a function of mean crystallite size and annealing temperature: Δ - as-prepared alloys; ○ – alloys annealed for 30 minutes at 400ºC, and ● – alloys annealed for 30 minutes at 700ºC. The coatings were produced by electrolysis from solution A.

Fig. 4. presents the temperature dependence of the relative magnetization of the as-prepared powder, milled powders and the same samples pre-annealed for 30 minutes at 440ºC. The relative magnetization is determined by the ratio of the magnetization of the tested sample at a temperature t to the magnetization of the as-deposited sample at 25ºC. The diagrams in Fig. 4 show that milled powders in the temperature range of 25ºC to 440ºC have a higher degree of magnetization compared to the as-deposited powders. During milling, amorphous phase crystallization produces an FCC phase with nanocrystal grains of an average size less than 11.1 nm. The reduction in the proportion of the amorphous phase enables the formation of larger magnetic domains and, hence, a higher degree of magnetization of the alloy.

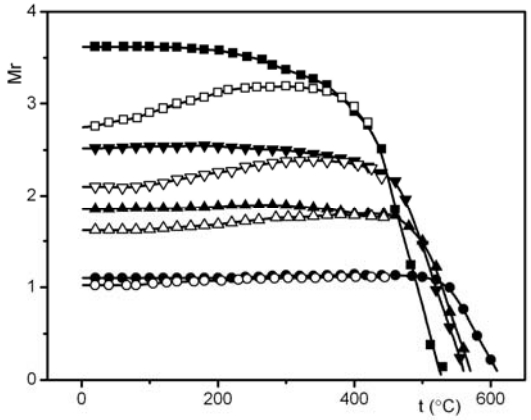

Fig. 4. Temperature dependence of relative magnetization: ○ – as-deposited powder; as-milled powders: Δ - 4 h, ∇ – 8h, □ – 12 h; powders pre-annealed for 30 minutes at 440ºC: ● – deposited and annealed powder, ▲ – powder milled for 4h and annealed, ▼ – powder milled for 8 h and annealed, and ■ – powder milled for 12 h and annealed. The powders were obtained by electrolysis from solution A at 500 $mAcm^{-2}$. Heating rate was 30ºC min^{-1}.

The relative magnetization of the as-prepared and as-milled powders does not significantly change during heating in the temperature range between room temperature and 80ºC. This indicates that in this temperature range no significant structural relaxation takes place. With an increase in temperature in the range of 80 - 440ºC, magnetization increases, reaching maximum at a certain temperature, but decreases thereafter with a further increase in temperature. The temperature of the magnetization maximum depends on alloy milling time. The longer the milling time, the lower the temperature of the maximum.

The magnetization of the pre-annealed samples does not change during heating from 25º to temperature Tc, indicating that during annealing for 30 minutes at 440ºC the alloy undergoes irreversible structural relaxation. The cooled samples pre-annealed at temperatures below 440ºC exhibit lower magnetization at 25ºC compared to samples pre-annealed at 440ºC. This suggests that during annealing at temperatures lower than 440ºC only partial structural relaxation occurs in the alloy powder. At temperatures above Tc, the magnetization of the alloy decreases abruptly with increasing temperature. The decrease is due to the change in the orientation of magnetic domains through the effect of heat.

Fig. 5. presents the relative magnetization of the as-prepared and annealed samples, the mean crystal size and the relative integral of X-ray diffraction peak intensities as a function of milling time. The relative magnetization is determined by the ratio of the magnetization of the tested sample at 25ºC and that of the as-deposited sample, also at 25ºC.

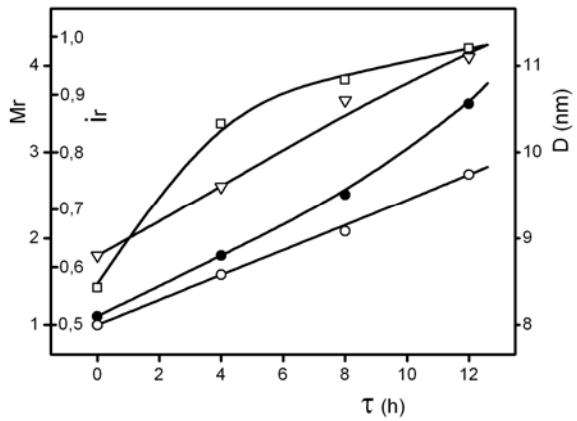

Fig. 5. Relative magnetization of: ○ – as-deposited samples, ● – samples annealed for 30 minutes at 440ºC; ∇ – mean size of non-annealed crystallites, and □ – the relative integral of FCC X-ray diffraction peak intensities, I_r, of non-annealed samples as a function of milling time. The powders were obtained by electrolysis from solution A at 500 mAcm^{-2}.

During annealing at temperatures above 440ºC, the alloy undergoes amorphous phase crystallization and crystal grain growth of the FCC phase of the solid solution of iron and tungsten and nickel. These structural changes cause changes in the magnetization and Curie temperature. Fig. 6. presents the temperature dependence of the relative magnetization of the as-deposited samples, as-prepared samples milled for 12 h and samples milled for 12 h followed by annealing at 440ºC and 600ºC.

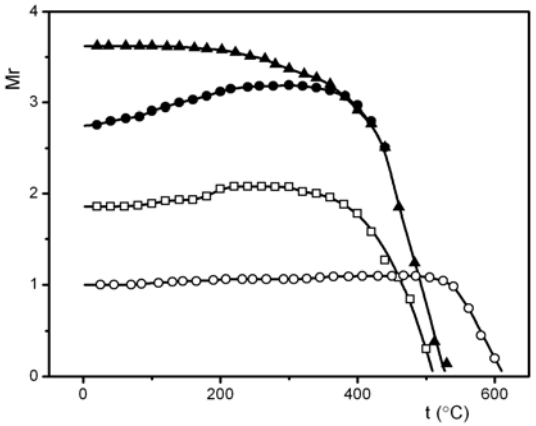

Fig. 6. Temperature dependence of the relative magnetization of: ○ – as-deposited sample; ● – sample milled for 12 h; ▲ – sample milled for 12 h and annealed for 30 minutes at 440ºC, □ – sample milled for 12 h and annealed for 30 minutes at 600ºC. The powder was obtained from solution A at 500 mAcm^{-2}. Heating rate was 30ºC min^{-1}.

The Fig. 6. shows that the sample annealed at 600ºC has a considerably lower magnetization and a lower Curie temperature compared to the as-milled sample and the sample milled and annealed at 440ºC. This also serves as a confirmation of the finding that the formation of large sized crystal grains during annealing at 600ºC causes a reduction in magnetization due to the impeded orientation of magnetic domains and decreased mobility of their walls. Due to the high proportion of the amorphous phase, the magnetization of the as-deposited sample is lower than that of the milled sample annealed at 600ºC. The increase in the mean size of FCC crystallites of the solid solution of iron and tungsten in nickel shifts the Curie temperature towards lower values.

The results show that an appropriate choice of deposition current density, milling time and annealing temperature can lead to nickel-iron-tungsten alloys with a low tungsten content (>1.5wt.%) and specific magnetic characteristics.

The tungsten content of the alloy affects its microstructure and morphology and, to a significant extent, its magnetic properties. Fig. 7. presents the temperature dependence of the relative magnetization of $Ni_{65}Fe_{24}W_{11}$ alloy electrodeposited from solution B at 500 $mAcm^{-2}$[13].

As shown in Fig. 7, during the first annealing up to 50ºC, there is no significant change in the relative magnetization, which suggests that no significant structural change takes place in the alloy in this temperature range. During heating in the temperature range of 50 - 350ºC, the relative magnetization shows a gradual decrease. The Curie temperature is about 350ºC. This value is close to the value for pure nickel, $T_{c,Ni}$ = 358ºC. The reorientation of magnetic domains at relatively low temperatures suggests their low thermal stability. The wide temperature range in which magnetization is gradually decreased indicates the coexistence of magnetic domains that have different thermal stabilities. The high deposition current density and the high tungsten content in the alloy cause: large local inhomogeneities of nickel, iron and tungsten contents (as determined by EDS point analysis); a high proportion of the amorphous phase and small crystal grains of the FCC phase with a high number of chaotically distributed dislocations and a high level of internal microstrain. Such a structure results in magnetic domains that exhibit different degrees of relatively low thermal stability and in alloys that have a considerably lower magnetization as compared to that of the alloys obtained at low current densities with a low tungsten content used (>1.5 mol%) [38]. The curves of the temperature dependence of the relative magnetization obtained during the second, third and fourth heatings in the temperature range of 50 - 425ºC show several waves. The coexistence of these waves suggests the existence of different sets of domains. The domains making up one set have approximately the same chemical composition and the same structure and, hence, the same thermal stability. The domains with higher iron contents have a higher Curie temperature.

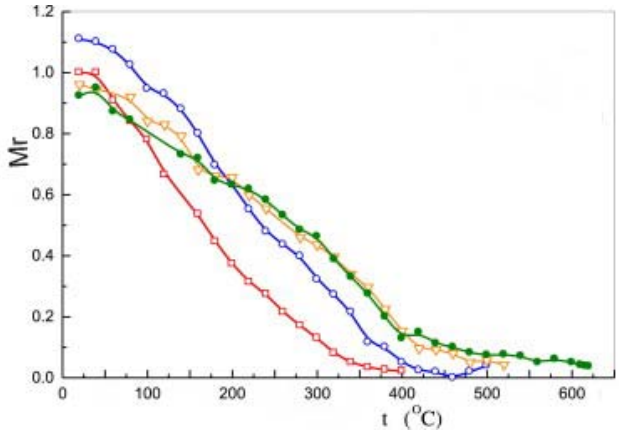

Fig. 7. Temperature dependence of the relative magnetization of $Ni_{65}Fe_{24}W_{11}$ alloy: □ – first heating; ○ – second heating; ∇ – third heating, and ● – fourth heating. The alloy powder was produced by electrolysis from solution B at 500 $mAcm^{-2}$ and at t=65ºC. Heating rate was 30ºC min^{-1}[13].

After the first annealing up to 400ºC, the relative magnetization of the alloy cooled at room temperature is increased by approximately 12% and the Curie temperature is increased by about 75ºC (Tc=425ºC). This is the result of structural relaxation taking place during the first annealing in amorphous phase clusters and FCC crystal grains of the solid solution of iron and tungsten in nickel. After the second heating to 500ºC, the alloy was cooled and, then,

heated for the third time to 525ºC. Then, it was cooled again and subjected to the fourth heating up to 625ºC. The curves obtained during the third and fourth annealings show that the relative magnetization of the alloy cooled at 25ºC is by about 5% and 8% lower than that of the as-prepared alloy. The decrease in magnetization at room temperature after the second and third annealings is caused by the crystallization of the amorphous portion of the powder and by crystal grain growth of the FCC-structured solid solution. As shown in Fig. 5., the increase in the number of annealings results in curves with more pronounced waves. During annealing, nickel and iron atoms diffuse and occupy energetically more stable sites, while forming different sets of clusters and crystal grains. Particles within the same set exhibit similar microstructures and chemical compositions. Similar particles build magnetic domains that have approximately the same thermal stability. The results show that the relatively high tungsten content of 11 wt. % in the $Ni_{61}Fe_{24}W_{11}$ alloy reduces the magnetization of the alloy and the thermal stability of magnetic domains.

Changes in the microstructure of nickel-iron-tungsten alloy electrodeposits during annealing and milling induce changes in their electrical resistivity. The as-obtained milled $Ni_{87.3}Fe_{11.3}W_{1.4}$ electrodeposits were heated to 550ºC while electrical resistivity was measured. Fig. 8. shows the temperature dependence of the electrical resistance of the as-obtained and milled $Ni_{87.3}Fe_{11.3}W_{1.4}$ electrodeposit [14].

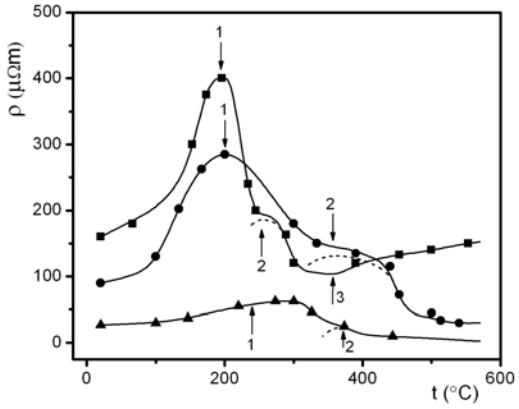

Fig. 8. Temperature dependence of electrical resistivity: ■ – as-deposited powder; ● – powder milled for 8 hours, and ▲ – powder milled for 12 hours. Heating rate 30ºC min^{-1}. The deposit was obtained from solution A at j=500 $mAcm^{-2}$[14].

As shown in the Fig., the resistance is the highest for the as-obtained deposit and lowest for the powder milled for 12 hours. The resistance decreases with increasing milling time. All diagrams show a maximum and a shoulder. The decrease in electrical resistivity after the maximum causes structural relaxation. In the range between the temperature of the maximum and the temperature of the shoulder, short-range ordering (most probably) takes place mostly in the amorphous phase. The decrease in resistivity after the shoulder is most likely the result of dominant microstructural relaxation changes in nanocrystals. Due to the relatively rapid heating and short time in the temperature range of 400 - 550ºC, there was no substantial crystallization of the amorphous phase and, accordingly, there was no significant decline in specific electrical resistance in this range.

Fig. 9. illustrates specific electrical resistance at 25º, 200ºC and 500ºC and the mean crystallite size as a function of the relative integral of peak (111), (200), (220) and (311) intensities in adequate X-ray diffractograms. The value of the relative integral of peak intensities for the sample heated for 60 minutes at 600ºC was taken as the reference value i.e. 1. It was assumed that the values of the mean crystallite size and the proportion of the amorphous phase during a short period of heating at 500ºC showed no significant change. The

diagrams show that electrical resistivity is higher in (structurally non-relaxed and relaxed) alloys that have a higher amorphous phase content.

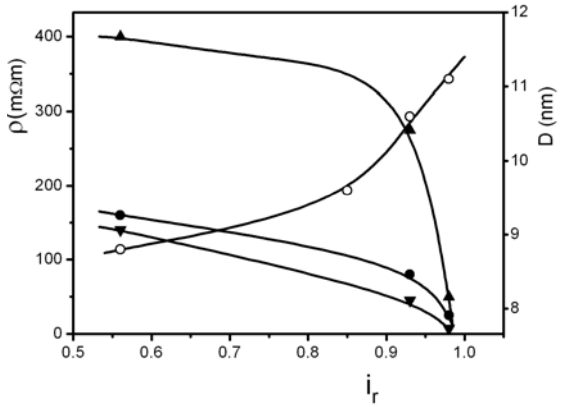

Fig. 9. Specific electrical resistance at ● - 25ºC, ▲ - 200ºC and ▼ - 500ºC, and ○ – mean crystallite size as a function of the relative integral of peak (111), (200), (220) and (311) intensities of the deposits obtained from solution A at j=500 mAcm^{-2}.

Short-range ordering during the relaxation causes an increase in the electron density of states in the conduction band at the Fermi level and an increase in the mean free path of electrons [13-16, 22, 23, 28, 42, 45]. During the process, the dipole moments, $\vec{p}$, of certain nanoparticles seem to be more uniformly oriented [22, 46]. The increase in the electron density of states, n, at the Fermi level, the increase in the mean free path of electrons, $\vec{l}$, and more uniform orientation of dipole moments, $\vec{p}$, cause a decline in electrical resistivity (an increase in electrical conductivity, $\vec{\sigma}$) during the structural relaxation, according to the equation:

$$\vec{\sigma} = \frac{ne^2\vec{l}}{\vec{v}} \quad \text{……. (1)}$$

where: $\vec{v}$ – average electron velocity. The dipole moment is expressed as:

$$\vec{p} = \vec{l} \cdot e \quad \text{……. (2)}$$

Combining equations (1) and (2) gives the expression:

$$\vec{\sigma} = \frac{ne\vec{p}}{\vec{v}} \quad \text{……. (3)}$$

The dipole moment has two contributions:

$$\vec{p} = \overrightarrow{p_{el}} + \overrightarrow{p_{ph}} \quad \text{……. (4)}$$

where: $\overrightarrow{p_{el}}$ – the electron part of the dipole moment, which is little dependent on temperature, and $\overrightarrow{p_{ph}}$ – the phonon part of the dipole moment which is much dependent on temperature, since bosons are sensitive to the electron-phonon and electron-magnon anharmonic interactions [16, 22, 46].

Specific electrical resistance is both directly and indirectly affected by milling. The direct effect is due to the effect of thermal energy coming from the transformation of mechanical energy during milling. Through the effect of thermal energy, the amorphous phase

in the alloy is transformed into a crystalline FCC phase and existing FCC crystal grains grow as the mean microstrain value and minimum density of chaotically distributed dislocations are decreased. These processes lead to a reduction in both peak intensity and shoulder intensity and cause a shift in the temperature of the peak maximum and shoulder temperature towards higher temperatures (Fig. 8). The indirect effect of milling is due to the evolvement of small particles which make better contact during pressing.

Under adjusted electrodeposition conditions and through subsequent thermal treatment of the deposit, alloys exhibiting different chemical compositions, morphologies and microstructures and, hence, different mechanical, corrosion and catalytic properties are obtained. This paper examines the effect of electrodeposition current density and annealing temperature on the hardness of nickel-iron-tungsten alloy coatings electrodeposited from solution A on mild steel substrate. Fig. 10. presents the hardness of the as-prepared annealed coatings, the tungsten content and the mean crystallite size as dependent on electrodeposition current density.

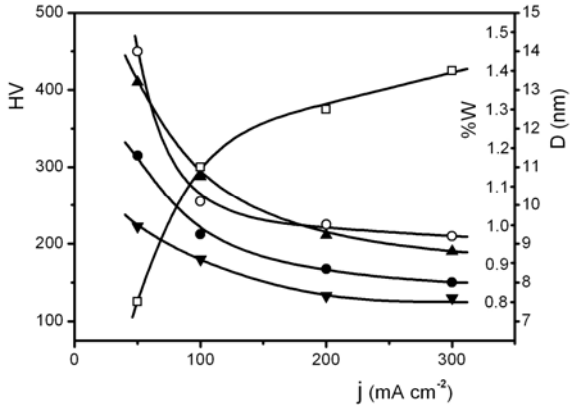

Fig. 10. Dependence of: □- tungsten content, ○ – mean crystal size, and ●, ▲, ▼ – hardness (of ● – as-prepared coating annealed for 60 minutes at: ▲ - 300ºC and ▼ – 500ºC) on electrodeposition current density. The coatings were produced from solution A.

Fig. 10. shows that the as-prepared coatings annealed at 300ºC and 500ºC obtained at higher current densities in the current density range of 50 to 300 mAcm^{-2} exhibit lower hardness compared to the coatings obtained at lower current densities. The hardness of nickel-iron-tungsten alloys is dependent on tungsten content, crystal grain size and amorphous phase content. The facts that an increase in tungsten content in nickel-iron-tungsten alloys increases their hardness and that the tungsten content is slightly increased in the tested samples obtained at higher current densities while their hardness is decreased suggest that the hardness of the electrodeposited alloys is dominantly affected by mean crystal size and amorphous phase content (Fig. 10). As the mean crystal size decreases up to a critical value, the hardness of the alloy is increased (the direct Hall-Petch relation). In alloys with a mean crystal size less than critical, their hardness decreases with decreasing crystal size (the inverse Hall-Petch relation) [9, 17, 47-49]. The hardness of the alloy, with crystal grains higher than the critical value, is determined by dislocation motion. The reduction in crystal grain size increases the proportion of grain boundaries in the alloy, thus impeding dislocation motion and increasing the hardness of the alloy. The hardness of the alloy with crystal grains less than the critical value is determined by grain boundary sliding. The hardness of the amorphous phase is low [7, 50]. The thickness of the sliding planes increases with decreasing crystal grain size and increasing amorphous phase content. The increased thickness of the plane causes a decrease in hardness [47]. The coatings formed at current densities of 50 to 300 mAcm^{-2} have an average crystal

size smaller than the critical size. The coatings with such crystal grains obtained at higher current densities have a greater thickness of sliding planes and, hence, lower hardness.

The hardness of the coatings is significantly dependent on annealing temperature (Fig. 11). With the increase in annealing temperature up to about 300ºC, the hardness of the coatings electrodeposited at current densities of 50 to 300 $mAcm^{-2}$ is increased. A further increase in annealing temperature results in decreased hardness.

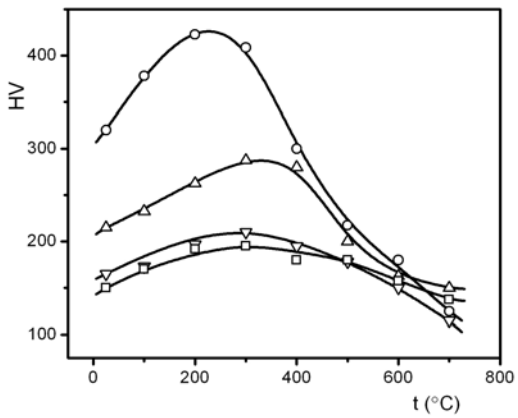

Fig. 11. Hardness of nickel-iron-tungsten coatings obtained from solution A as a function of annealing temperature and deposition current density: ○ – 50 $mAcm^{-2}$, Δ – 100 $mAcm^{-2}$, ∇ - 200 $mAcm^{-2}$, and □ - 300 $mAcm^{-2}$[15].

During annealing at temperatures up to 300ºC, the increase in hardness is dominantly due to short-range ordering during which ordering and mean cluster size in the sliding plane are increased and, accordingly, grain boundary sliding is hampered.

Apart from short-range ordering, during annealing, the hardness of the alloy is increased by the removal of hydrogen [51], carbon and oxygen [44] incorporated during electrodeposition.

The decrease in alloy hardness with increasing annealing temperature at temperatures above 300ºC is due to a decrease in the level of remaining strain as well as due to larger crystal grains formed through amorphous phase crystallization. At temperatures above 400ºC, the dominant effect is produced by the formation of larger grains.

The results indicate that solution composition, solution temperature, deposition current density, annealing temperature and milling time determine the chemical composition, morphology and microstructure of electrodeposited nickel-iron-tungsten alloys and show the presence of a correlation between the microstructure and magnetic, electrical and mechanical properties. This suggests that the choice of appropriate synthesis and subsequent treatment conditions can help generate alloys that have pre-defined physicochemical properties.

4. Conclusion

Nanostructured nickel-iron-tungsten alloys were produced by electrodeposition from an ammoniacal citrate bath. The chemical composition and microstructure of the alloys were found to affect their hardness and magnetic and electrical properties. The magnetization of the alloys with a low tungsten content (< 1.4 wt.%) increases with increasing crystal grain size from 8.8 nm to 14.0 nm. The increase in magnetization is due to a reduction in the amorphous phase proportion and due to a decrease in the density of chaotically distributed dislocations. Annealing the coatings at temperatures lower than 400ºC results in increased magnetization since certain atoms located at higher energy levels cross energy barriers through the effect of

thermal energy and reach lower energy levels where their 3d and 4s orbitals overlap more effectively with the same type of orbitals of neighboring atoms, thus increasing the value of the exchange integral, the electron density of states at the Fermi level and the mean free path of electrons. This enhances the mobility of magnetic domain walls and facilitates the orientation of these domains in the external magnetic field. In the temperature range between 400ºC and 700ºC, the magnetization decreases with increasing temperature since amorphous phase crystallization results in the formation of larger crystal grains of the FCC phase which impede the orientation of certain magnetic domains and reduce the shift of walls of already oriented domains. During the 12-hour milling of the as-deposited $Ni_{87.3}Fe_{11.3}W_{1.4}$ alloy with a mean crystal grain size of 8.8 nm, the resulting heat causes amorphous phase crystallization and FCC crystal grain growth to 11.1 nm accompanied by a decrease in the density of chaotically distributed dislocations, leading to an increase in the magnetization of the alloy. During the annealing of the milled alloys up to 440ºC, structural relaxation and short-range ordering take place, resulting in an increase in magnetization. At higher temperatures, the crystallization of the amorphous phase in the milled alloy produces larger FCC crystal grains, inducing a decrease in the magnetization of the alloy and a shift of the Curie temperature towards lower temperatures.

The alloys having higher tungsten content, $Ni_{65}Fe_{24}W_{11}$ have large local inhomogeneities of nickel, iron and tungsten contents, a high proportion of the amorphous phase, and small crystal grains of the FCC phase with a high number of chaotically distributed dislocations and a high internal microstrain level. Such a structure results in different magnetic domains that exhibit relatively low thermal stability, and low magnetization of the alloy. The domains with higher iron content have a higher Curie temperature.

Amorphous phase crystallization and FCC crystal grain growth during the milling of $Ni_{87.3}Fe_{11.3}W_{1.4}$ alloys with a mean crystal size of 8.8 nm cause a decline in the specific electrical resistance of the alloys. Electrical resistivity decreases with increasing annealing temperature at temperatures below the crystallization temperature due to structural relaxation during which the electron density of states at the Fermi level and the mean free path of electrons are increased and the dipole moments of certain nanoparticles are more uniformly oriented.

The hardness of the nickel-iron-tungsten alloy coatings with a tungsten content less than 1.4wt.% obtained at the current densities between 50 and 300 $mAcm^{-2}$ decreases with the decrease in the mean crystal grain size of the FCC phase from 14.0 nm to 9.2 nm. Given that the mean crystal grain size of these alloys is below the critical value, their hardness decreases with decreasing crystal grain size due to an increase in the thickness of the sliding plane composed of an amorphous phase. During annealing up to 300ºC, the alloys undergo structural relaxation, during which short-range ordering and the mean cluster size in the siding plane are increased, thus impeding the sliding of grain boundaries and, hence, increasing the hardness of the alloys. At temperatures from 300 to 500ºC, the decrease in hardness mostly causes a reduction in the remaining strain, and at temperatures above 500ºC the formation of the FCC phase with a relatively high mean crystal size is observed.

A correlation was found between the microstructure of the nickel-iron-tungsten alloy and its magnetic and electrical properties and hardness.

Acknowledgments

The authors acknowledge the financial support provided by the Ministry of Education and Science of the Republic of Serbia through Project Ref. No. 172057.

5. References

1. N.Atanassov, K.Gencheva, and M.Bratoeva, Plat. Surf. Finish., 84, 67 (1997).
2. M.Donten, H.Cesiulis, and Z.Stojek, Electrochim. Acta, 45, 3389 (2000).
3. Z.He and T.H. Courtney, Mater. Sci. Eng. A, 346, 141 (2003).
4. S.H. Hong and H.J. Rya, Matr. Sci. Eng. A, 344, 253 (2003).
5. Z.W. Zhang, J.I.E. Zhou, S.Q. Xi, G. Ran, P.L. Li, and W.X. Zhang, J.Alloy. Compd., 370, 186 (2004).
6. Z.W.Zhang, J.I.E. Zhou, and S.Q.Xi, Mater. Sci. Eng. A, 379, 148 (2004).
7. K.R.Sriraman, S.G. Raman, and S.K. Seshadri, Mater. Sci. Eng. A, 418, 303 (2006).
8. K.R.Sriraman, S.G. Raman, and S.K. Seshadri, Mater. Sci. Technol., 22, 14 (2006).
9. F.He, J.Yang, T.Lei, and C.Gu, Appl. Surf. Sci, 253, 7591 (2007).
10. P. Esther, C.JosephKennady, P.Saravanan, and T.Venkatachalam, J. Non-Oxide Glasses, 1, 301 (2009).
11. A. Mondal, A. Upadhyaya, and D. Agrawal, J. Alloy. Compd., 509, 301 (2011).
12. M. Banerjee, A. Singh, A.K. Majumdar, and A. K. Nigam, J. Phys.: Condens. Matter., 23, 3060004 (2011).
13. L. Ribić-Zelenović, N. Ćirović, M. Spasojević, N. Mitrović, A. Maričić, and V. Pavlović, Mater. Chem. Phys., 135, 212 (2012).
14. M. Spasojević, L. Ribić-Zelenović, N. Ćirović, P. Spasojević, and A. Maričić, Sci. Sinter., 44, 197 (2012).
15. M. Spasojević, N. Ćirović, L. Ribić-Zelenović, P. Spasojević, and A. Maričić, J. Electrochem. Soc. 161(10) D1-D7 (2014).
16. Z. Vuković, P. Spasojević, M. Plazinić, J. Živanić, M. Spasojević. J. Optoelectron. Adv. Mater., 16, 985 (2014).
17. S. J. Mun, M.S. Kim, T. H. Yim, J. H. Lee, and T. Kang, J. Electrochem. Soc., 157, D177 (2010).
18. V. B. Singh, Surf. Technol., 7, 443 (1978).
19. A. R. Despić and K.I. Popov, Modern Aspects of Electrochemistry, vol. 7, Plenum Press, New York, (1972).
20. K. I. Popov and M.G. Pavlović, in Modern Aspects of Electrochemistry, Vol. 24, B. E. Conway, J. O'M. Bockris, and R. E. White, Editors, p. 299, Plenum, New York, 1973.
21. M. G. Pavlović, Lj. J. Pavlović, E.R. Ivanović, V. Radmilović, and K.I. Popov, J. Serb. Chem. Soc., 66, 923 (2001).
22. L. Ribić-Zelenović, M. Spasojević, and A. Maričić, Mater. Chem. Phys., 115, 347 (2009).
23. L. Ribić-Zelenović, M. Spasojević, A. Maričić, and M.M. Ristić, Sci. Sinter., 41, 175 (2009).
24. L. M. Chang, Z. T. Wang, S. Y. Shi, and W. Liuy, J. Alloy. Compd., 509, 1501 (2011).
25. M. A. Oliver-Tlentino, E. M. Arce-Estrada, C. A. Córtes-Escobedo, A. M. Bolarin-Miro, F. Sánches-De Jesus, R. DeG. Gonzales-Huerta, and A. Manzo-Robledo, J. Alloys. Compd., 536S, S245 (2012).
26. L.X. Phua, N.N. Phuoc, and C.K. Ong, J. Alloy. Compd., 520, 132 (2012).
27. L. D. Rafailović, C. Gammer, C. Rentengerger, P. Angerer, and H. P. Karnthaler, J. Alloy. Compd., 543, 167 (2012).
28. M. Spasojević, L. Ribić-Zelenović, and A. Maričić, Sci. Sinter., 43, 313 (2011).
29. E. J. Podlaha and D. Landolt, J. Electrochem. Soc., 143, 893 (1996).
30. E. J. Podlaha and D. Landolt, J. Electrochem. Soc., 144, 1672 (1997).
31. D. Landolt, E. J. Podlaha, and N. Zech, Zh. Phys. Chem., 208, 167 (1999).

32. A. Maričić, M. Spasojević, L. Rafailović, V. Milovanović, and L. Ribić-Zelenović, Mater. Sci. Forum, 453, 411 (2004).
33. L. Ribić-Zelenović, L. Rafailović, M. Spasojević, and A. Maričić, Phys. B, 403, 2148 (2008).
34. E. Chassaing, K. Vu Quang, and R. Wiart, J. Appl. Electrochem, 19, 839 (1989).
35. O. Younes and E. Gileadi, Electrochem. Solid State Lett., 3, 543 (2000).
36. O. Younes, L. Zhu, Y. Rosenberg, Y. Shacham-Diamond, and E. Gileadi, Langmuir, 17, 8270 (2001).
37. M. D. Obradović, R. M. Stevnović, and A.R. Despić, J. Electroanal. Chem., 552, 185 (2003).
38. G. Herzer, IEEE Trans. Magn., 25, 3327 (1989).
39. J. D. Bernal, Nature, 185, 68 (1960).
40. S. Roth, H. Grahl, J. Degmova, N. Schlorke-de Boer, M. Stoica, J. M. Borrego, A. Conde, and N. M. Mitrović, J. Optoel, Adv. Mater., 4, 199 (2002).
41. N. Mitrović, J. Magn. Magn. Mater., 262, 302 (2003).
42. L. Ribić-Zelenović, L. Rafailović, A. Maričić, and M. Spasojević, J. Optoel. Adv. Mater., 9, 2681 (2007).
43. K.E. Heusler, D. Huerta, J. Electrochem. Soc., 136, 65 (1989).
44. M. Donten, J. Solid State Electrochem., 3, 87 (1999).
45. M.Spasojevic, L. Ribic-Zelenovic, A. Maricic, P. Spasojevic, Powd. Techn., 254, 439 (2014).
46. K. Nouneh, I. V. Kityk, R. Viennois, S. Benet, K. J. Plucinski, S. Charar, Z. Golacki, S. Paschen, J. Phys. D: Appl. Phys. 38, 965 (2005).
47. T. Yamaski, Scripta Mater., 44, 1497 (2001).
48. H. Conrad, J. Narayan, Scripta Mater., 42, 1025 (2000).
49. Y.Wu, D. Chang, D. Kim, S. Kwon, Surf. Coat. Technol., 173, 259 (2003).
50. T. Yamasaki, P. Schlo, K. Ehrlich, Y. Ogino, Nanostruct. Mater., 10 (1998) 375.
51. Y.D. Gamburg, E. N. Zakharov, Russ. J. Electrochem., 44, 736 (2008).

Садржај: *Из амонијачно-цитратног купатила депоноване су наноструктурне легуре никла, гвожђа и волфрама. Садржај волфрама у легури варирао је од 0.8 мас% до 11 мас% а величина кристалних зрна FCC фазе чврстог раствора гвожђа и волфрама у никлу од 14 nm до 3.3 nm. Садржај аморфне фазе у легури расте са смањењем величине кристалних зрна. Са порастом садржаја аморфне фазе опада магнетизација, специфична електрична проводљивост и тврдоћа легура. Одгревањем легура до температуре кристализације у легури се одвија структурна релаксација током које се уређује структура на кратко праћена смањењем густине хаотично распоређених дислокација и унутрашњих микронапрезања што узрокује повећање вредности интеграла измене, густине стања електрона у близини Ферми нивоа, средње дужине слободног пута електрона, уређености и средње димензије кластера у равни клизања и униформнију оријентацију диполних момената појединих наночестица. Наведене промене узрокују: а) већу покретљивост зидова магнетних домена, лакше усмеравање домена у спољашњем магнетном пољу и повећање магнетизације; б) смањење специфичне електричне отпорности и в) отежано клизање граница зрна и повећање тврдоће легура.*

Одгревањем легура на температурама вишим од 400ºC одвија се кристализација аморфне фазе и формирање већих кристалних зрна FCC фазе уз смањење густине хаотично распоређених дислокација и унутрашњих микронапрезања.

Настанак већих кристалних зрна узрокује смањење тврдоће и специфичне електричне отпорности и отежава усмеравање појединих магнетних домена и померање зидова већ усмерених домена и тако смањује магнетизацију.

Топлота ослобођена током млевења легуре $Ni_{87.3}Fe_{11.3}W_{1.4}$ са кристалним зрнима FCC фазе просечне димензије 8.8 nm узрокује кристализацију аморфне фазе, раст кристалних зрна FCC фазе и повећање магнетизације легуре.

Легура са релативно великим садржајем волфрама (11 mac%) имају нехомоген састав, велики удео аморфне фазе и кристална зрна FCC фазе просечне димензије 3.3 nm. Последица ове микроструктуре је егзистенција магнетних домена различите и релативно мале термичке стабилности и релативно мале магнетизације легуре.

Кључне речи: *наноструктурна легура, FCC фаза, специфична електрична отпорност, магнетизација*